THE JOURNAL OF PHYSICAL CHEMISTRY B

Article

Cite This: J. Phys. Chem. B XXXX, XXX, XXX−XXX

pubs.acs.org/JPCB

Dynamics of Water Molecules and Ions in Concentrated Lithium Chloride Solutions Probed with Ultrafast 2D IR Spectroscopy

Rongfeng Yuan and Michael D. Fayer*

Department of Chemistry, Stanford University, Stanford, California 94305, United States

Supporting Information

ABSTRACT: Water and ion dynamics in concentrated LiCl solutions were studied using ultrafast 2D IR spectroscopy with the methyl thiocyanate (MeSCN) CN stretch as the vibrational probe. The IR absorption spectrum of MeSCN has two peaks, one peak for water associated with the nitrogen lone pair of MeSCN (W) and the other peak corresponding to Li^+ associated with the lone pair (L). To extract the spectral diffusion (structural dynamics) of W and L species, we developed a method that isolates the peak of interest by subtracting the 2D Gaussian proxies of multiple interfering peaks. Center line slope data (normalized frequency−frequency correlation function) for 2D bands from the W and L are fit with triexponential functions. The fastest component (1.1−1.6 ps) is assigned to local hydrogen bond length fluctuations. The intermediate timescale (~4.0 ps) corresponds to the hydrogen bond network rearrangement. The slowest component decays in ~40 ps and corresponds to ion pair and ion cluster dynamics. The very similar W and L spectral diffusion indicates that the motions of the water and ions are strongly coupled. Orientational relaxations of the W and L species were extracted using a new method to eliminate the effects of overlapping peaks. The results show that MeSCN bound to water undergoes orientational relaxation significantly faster than MeSCN bound to Li^+. The orientational and spectral diffusion results are compared. A Stark coupling model is used to extract the root mean square average electric field caused by the ion clouds along the CN moiety as a function of concentration.

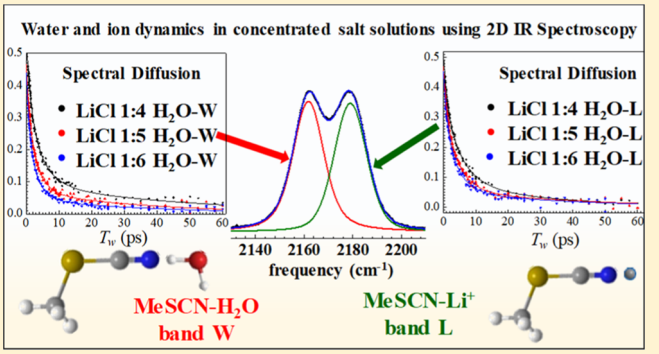

1. INTRODUCTION

Characterizing aqueous electrolyte solutions is important because of their ubiquity in biological systems, chemistry, and industrial applications such as fuel cells and water desalination. The solvation structure of ions and the dynamics of the water hydrogen bond network are among the interesting aspects of salt solutions. Many techniques have been applied to elucidate these issues, including NMR, Raman spectroscopy, X-ray and neutron diffraction, and molecular dynamics (MD) simulations.[1−8] Ultrafast infrared (IR) spectroscopies can probe ground-state water and ion dynamics with femtosecond temporal resolution, while the absorption spectra can provide specific molecular interaction information in aqueous salt solutions.[9−20]

Recently, concentrated electrolyte solutions, sometimes referred to as "water-in-salt" electrolyte solutions, have drawn attention because of their potential applications in battery technology.[21,22] In these solutions, the hydrogen bond network among water molecules is severely disturbed and should not be viewed as just a slower version of dynamics in pure water. The ions cannot be fully solvated by water molecules and form pairs and clusters. The crowded ionic environment, which produces strong electric fields, will restrain the motions of water molecules. Previous publications have shown that even though different ions may speed up or slow down hydrogen bond rearrangement dynamics in low concentration, water dynamics always slows down in solutions with high ionic concentrations.[23−27] This slower dynamics is a commonality among ion types, and understanding the nature of this concurrence promises deeper understanding of water−ion interactions.

Lithium chloride (LiCl) is a salt that is widely used as a model system for concentrated salt solution because of its high solubility and easy accessibility. Numerous experiments and simulations have been performed on LiCl solution to examine its structure and dynamics.[5,28−35] Previously, we reported the application of the CN stretch of methyl thiocyanate (MeSCN) as a probe to interrogate ion−molecule complex formation and dissociation dynamics in concentrated lithium chloride (LiCl) solution.[36] In these systems, we observed the dissociation and association dynamics between MeSCN and Li^+, requiring the concomitant association and dissociation of water, the rate constants of which are largely independent of viscosity or ionic strength. At the same time, we did observe that the water-associated MeSCN (W) and the Li^+-associated MeSCN (L) both experience slower reorientational relaxation as the viscosity increases though W always has faster reorientation

Received: June 24, 2019
Revised: August 2, 2019
Published: August 11, 2019

DOI: 10.1021/acs.jpcb.9b06038
J. Phys. Chem. B XXXX, XXX, XXX−XXX

dynamics than L for several concentrations. These results contain a detailed dynamical picture of ion−molecule interactions. However, water and ion dynamics, such as hydrogen bond rearrangement timescales or ion cluster dynamics, are not contained in the chemical exchange dynamics. Spectral diffusion of the two species, which can be obtained from band shape analysis of the 2D spectra, shed light on these issues. We have shown that the CN stretch of MeSCN accurately reports on hydrogen bond dynamics in pure water,[36] indicating that it should also be a good probe in salt solutions. Yet, the analysis of spectral diffusion data is not straight forward because of the significant overlap of the 2D bands.

Here, we report a new method that greatly decreases the aberration of 2D band shape analysis caused by overlapping bands. We applied this method to extract the spectral diffusion of the CN stretch when the CN is associated with water and Li^+. In addition, we developed a method to extract reorientation dynamics, inspite of the overlapping peaks, using polarization-selective 2D spectra. This method was applied and generated more rigorous description of the orientational relaxation than previously reported.[36] These experiments provide a comprehensive description of ion and water dynamics in concentrated LiCl solutions.

2. RESULTS AND DISCUSSION

2.1. Band Shape Analysis. The experimental details have been reported previously.[36] Here, we include only a brief introduction to the 2D IR spectroscopy.[36] There are four pulses in the pulse sequence. The first two pulses (pump pulses) label and store the initial frequencies, ω_τ. After a waiting time T_w, the third pulse (probe pulse) induces the emission of vibrational echo pulse, the fourth pulse, and the probe pulse also acts as the local oscillator for the echo. Through heterodyne detection, the latter two pulses read out the final frequencies, ω_m. A 2D IR spectrum, with ω_τ and ω_m as horizontal and vertical axes, reports on the correlation between ω_τ and ω_m after frequency evolution of the period T_w. Frequency evolution will sample all the frequencies in the inhomogeneously broadened absorption band after a sufficiently long time. The frequencies evolve because the liquid structure changes with time, causing intermolecular interactions, which in part determine the vibrational frequencies, to change. This process is called spectral diffusion. Spectral diffusion leads to gradual decorrelation between initial and final frequencies. This decorrelation process can be characterized by frequency−frequency correlation function or FFCF.[37,38] FFCF is defined as the probability that an oscillator with an initial frequency will have the same frequency at time t later, averaged over all initial frequencies in the inhomogeneous spectral distribution.

For a single 2D band that has a time-dependent shape because of spectral diffusion, the time-dependent correlation can be extracted using the center line slope (CLS) method.[37,38] To calculate the CLS from the 2D spectrum at a given T_w, a series of slices parallel to the ω_m axis through the 2D spectrum in the region around the spectrum's center are obtained. Each slice is a 1D spectrum. The center line consists of the set of (ω_m, ω_τ) points that are the peaks of these 1D spectra, and the CLS is the slope of this line. The CLS(T_w), which is a plot of the slopes versus T_w, is the normalized FFCF.[37] The complete FFCF is typically modeled as a sum of exponentials with a Kubo line shape function[39,40] shown in eq 1; the decay constants provide a quantitative measure of timescales for the system's structural dynamics as reported by the vibrational probe.

$$C(t) = \langle \delta\omega(t)\delta\omega(0)\rangle = \sum_i \Delta_i^2 \exp(-t/\tau_i) \quad (1)$$

Here, $\delta\omega(t) = \omega(t) - \langle\omega\rangle$ is the instantaneous frequency fluctuation and $\langle\omega\rangle$ is the average frequency. The Δ_i are the frequency fluctuation amplitudes of each component, and the τ_i are the associated time constants.

The accuracy of the CLS(T_w) depends on the ability to determine the CLS at each T_w. For a single band on the diagonal with its associated 1−2 band below it, the method is robust.[38] Methods have been developed for two bands on the diagonal, which require knowing the CLS(T_w) of one of them.[41,42] In addition, it has been shown that when two bands on the diagonal overlap to a significant extent but not too much, the CLS(T_w) of each band can be obtained in the same manner as if they are single bands.[42] However, many systems are more complicated than those that have previously been treated. If the CLS(T_w) of both diagonal bands are unknown, and if there are several overlapping off-diagonal bands, the method presented here makes it possible to obtain accurate CLS(T_w), characterizing the dynamics.

Figure 1 shows the absorption spectra of the CN stretch of MeSCN in the three high-concentration LiCl solutions and in pure water. The three LiCl solutions have the ratios of ion pairs to water molecules of 1:4 (10.7 M), 1:5 (9.0 M), and 1:6 (7.7 M). The low-frequency peaks arise from water bound to the N lone pair of the CN moiety (W). These peaks for MeSCN in the concentrated LiCl solutions have essentially the same center frequency as in pure water, but they are somewhat broader. The spectra have been normalized at the peak frequency. The peaks at the higher frequency correspond to MeSCN populations that have a Li^+ bound to the N lone pair (L). Their amplitudes decrease relative to the W peaks as the LiCl concentration is reduced. The bands arising from W and L in the 2D IR spectrum appear as two peaks on the diagonal.

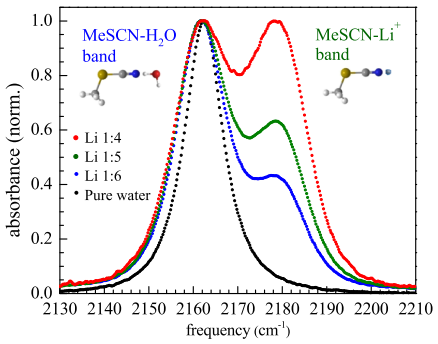

Figure 1. FT-IR absorption spectra of the CN stretch of MeSCN in the three high concentration LiCl solutions and in pure water. The three LiCl solutions have the ratios of ion pairs to water molecules of 1:4 (10.7 M), 1:5 (9.0 M), and 1:6 (7.7 M). (Adapted with permission from (*J. Phys. Chem. B* **2018**, *122*, 10582−10592). Copyright (2018) American Chemical Society).

In addition to the diagonal peaks from the W and L species, chemical exchange produces cross-peaks and 1−2 transitions produce additional peaks, which exacerbate the complexity of the spectra. Figure 2 shows 2D IR spectra for a 1:4 solution at three T_ws. In the top panel, the two peaks are well separated on

DOI: 10.1021/acs.jpcb.9b06038
J. Phys. Chem. B XXXX, XXX, XXX−XXX

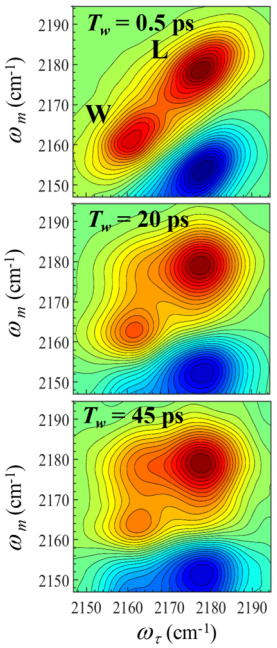

Figure 2. Experimental 2D spectra of MeSCN in LiCl 1:4 H_2O solution at three T_ws. As T_w increases, the band shapes of the diagonal peaks, especially W, are severely distorted by overlap with each other, exchange peaks, and 1−2 transition bands.

the diagonal, but the 1−2 blue (negative going) band from L distorts the shape to some extent of the band next to it from W. As time progresses in the next two panels, the spectra become more congested as the off-diagonal chemical exchange bands grow in.[36] In these circumstances, performing the CLS analysis on the bands from L and W as if the other bands are not present will not produce the correct CLS(T_w)s.

The absorption lines of the CN stretch of the probe MeSCN in water and LiCl solutions are symmetric.[36] Therefore, we are able to model the 2D spectral bands with symmetric functional forms. We take advantage of this feature and apply a new approach as a generalization of the method used by Giammanco et al.[41] In the prior work,[41] the authors scale-subtracted a single known interfering 2D band to isolate a second 2D band that was of interest. Here, although we do not know the band shape of either component, they can be approximated by two-dimensional (2D) Gaussian functions that were used to extract the peak volume in a previous publication.[36] The procedure is to minimize the interference from other bands by isolating the peak of interest by subtracting the 2D Gaussian function proxies of other interfering peaks from the 2D spectra.

The procedure detailed below is robust because many aspects of the spectrum are known. From the Fourier transform infrared (FT-IR) spectrum or the very short time 2D IR spectrum, the center positions of the two diagonal bands are known. Given the center positions of the diagonal bands, the center positions of the off-diagonal exchange bands are known. At short time (top panel of Figure 2), the anharmonicity can be measured by modeling the experimental 2D spectra with two 2D Gaussians for the red 0−1 bands and two 2D Gaussians for the blue 1−2 bands (only one of which is shown in Figure 2). With the centers of the 1−2 bands known, the positions of the 1−2 exchange peaks are known. In addition, the shapes of the off-diagonal exchange bands are related to the shapes of the diagonal bands. Within the harmonic approximation, the shape of the 1−2 band is the same as the shape of the corresponding 0−1 band. As the anharmonicity is small, ∼25 cm^{-1}, this is a reasonable approximation. Then, the 1−2 exchange bands obey the same shape relationship as the 0−1 off-diagonal bands. Therefore, in fitting the entire spectrum with 2D Gaussians, the number of fitting parameters is greatly reduced and the fits are highly constrained.

The 2D Gaussian function is given by

$$G(x,y) = A\ \exp\Bigg(-4\ln(2)\left(\left(\frac{(x-\omega_{1,0})\cos\theta + (y-\omega_{3,0})\sin\theta}{\Delta\omega_1}\right)^2 + \left(\frac{(y-\omega_{3,0})\cos\theta - (x-\omega_{1,0})\sin\theta}{\Delta\omega_3}\right)^2\right)\Bigg) \quad (2)$$

In this equation, x and y are variables on the ω_1 (ω_τ) and ω_3 (ω_m) axes, respectively. $\Delta\omega_1$ and $\Delta\omega_3$ are full-width-at-half-maximum (fwhm) on the ω_1 and ω_3 axes, respectively. θ is the tilt angle of the 2D Gaussian relative to the ω_1 axis. $\omega_{1,0}$ and $\omega_{3,0}$ are the peak center positions of each component on the 2D spectra. For diagonal components, $\omega_{1,0} = \omega_{3,0}$. For a single component, such as the diagonal band from W, $\Delta\omega_3$ will be relatively small at early T_w and, as spectral diffusion occurs, becomes larger at later T_ws. The tilt angle θ is related to the CLS and will become increasingly close to zero as T_w increases. Overall, there are six parameters (A, θ, $\omega_{1,0}$, $\omega_{3,0}$, $\Delta\omega_1$, and $\Delta\omega_3$) that define a single 2D Gaussian function. However, as discussed qualitatively above, the parameters of various peaks are correlated, which greatly decreases the number of free parameters in the fitting procedure.

First, peak positions $\omega_{1,0}$ and $\omega_{3,0}$ for diagonal peaks and exchange peaks in the 0−1 transition region are predetermined via linear FT-IR spectroscopy and are only allowed to vary a small amount (∼0.5 cm^{-1}) in the fitting program. For peak positions of the negative-going 1−2 transition, $\omega_{1,0}$ is also fixed. In terms of $\omega_{3,0}$, the anharmonicities were determined at early T_w when there is almost no exchange peak and the overall 2D spectrum can be fitted with only four 2D Gaussians (two for 0−1 diagonal peaks and two for 1−2 peaks). The anharmonicities are given little room to change when fitting 2D spectra at later T_ws.

Second, the amplitude A's are correlated between relevant peaks. First, the amplitudes A of every peak in the 1−2 transition region are fixed to the same values as the corresponding 0−1 transitions but with an opposite sign. The identity of the amplitudes is correct within the harmonic approximation, which is generally quite accurate. In practice, even when this correlation is not forced, the difference of A's between a 1−2 peak and its corresponding 0−1 is less than 10%. Second, the pairs of exchange peaks are the same amplitude because of the requirement of equilibrium.[36] With these two conditions, there are only three independent A's in an entire 2D spectra, two for the diagonal peaks, and one for the exchange peaks.

DOI: 10.1021/acs.jpcb.9b06038
J. Phys. Chem. B XXXX, XXX, XXX−XXX

Third, the band shape of a 1−2 transition is the same as the corresponding 0−1 transition, which means that the related parameters θ, $\Delta\omega_1$, and $\Delta\omega_3$, are also shared between them. (This statement is valid in most cases but it does have exceptions[43]). In addition, for the exchange peaks in general there is no correlation between ω_1 and ω_3;[44] then θ can be set to 0. The $\Delta\omega_1$ and $\Delta\omega_3$ of exchange peaks, should be fixed to the $\Delta\omega_1$ of the diagonal peak sharing its initial frequency ω_1 and the $\Delta\omega_3$ of the diagonal peak sharing its final frequency ω_3, respectively. Therefore, only the θ, $\Delta\omega_1$ and $\Delta\omega_3$ of the two diagonal peaks are free variables.

To summarize, with peak positions of all components essentially fixed, there are only 9 free variables to fit an entire 2D spectrum, three amplitudes and two sets of band shapes (θ, $\Delta\omega_1$, and $\Delta\omega_3$) for diagonal peaks.

As an example, a 2D spectrum of LiCl 1:5 H_2O solution at T_w = 40 ps is shown in Figure 3. The top and middle plots are

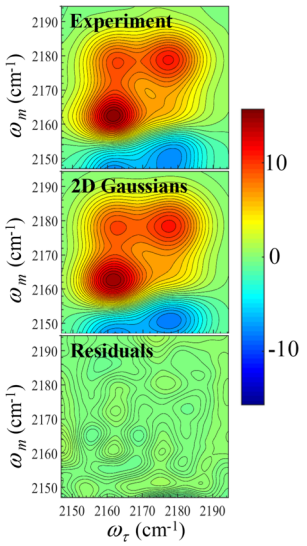

Figure 3. Illustration of the 2D subtraction method. The top panel is experimental data. The middle panel displays the 2D Gaussian reproduction of the experimental spectra. The bottom panel shows the results of subtracting the 2D Gaussian reproduction from the experimental data. The residuals are very small, showing the accuracy of the reproduction.

the experimental 2D spectrum and its corresponding reproduction with 2D Gaussian functions, respectively. The bottom plot is the residuals obtained by subtracting the calculated spectrum (middle plot) from the experimental spectrum (top plot). The residuals are very small, close to 0 (see color scale). This figure demonstrates the efficacy of the procedure; the 2D Gaussian functions are excellent approximations to the real band shapes.

The following procedure is used to remove the interference of other peaks so that CLS analysis can be performed. An example of extracting CLS of the W component in the 2D spectra of Figure 2 is presented in Figure 4. Figure 4 top row shows 2D Gaussian reproductions of the 2D spectra without the W diagonal component. To obtain these 2D Gaussian reproductions, the entire spectrum is fit as in Figure 3. Then the 2D Gaussian function that models the W species diagonal band at each T_w is removed while all other 2D Gaussian functions remain the same. These model spectra are subtracted from the experimental spectra (Figure 2) yielding the bottom panels in Figure 4, the experimental 2D spectra of the isolated W diagonal band. All spectra in Figure 4 share the same color scale. As can be seen, W components are isolated, and the noises of surrounding areas are very small. The CLS data is taken around the peak of the 2D spectra where the signal amplitude is the greatest. The small residual seen in Figures 4 and 3 will have a negligible impact on the band shape around the peak. It is important to note that the CLS is performed on the actual 2D experimental data, not on the 2D Gaussian reproductions. The reproductions are used to remove any distortions caused by the other bands. Detailed discussions about the various conditions under which this method is applicable are presented in Supporting Information.

2.2. Chemical Exchange-Induced Spectral Diffusion.

As discussed above, the CLS(T_w) obtained from the 2D spectra is the normalized FFCF, which quantifies spectral diffusion. Without chemical exchange, the CLS(T_w) characterizes the structural dynamics of the medium as reported by the vibrational probe. When chemical exchange occurs, there is also a contribution to spectral diffusion from the chemical exchange. Consider the W diagonal peak for example, the diagonal population can be divided into two ensembles. One ensemble of molecules at a given T_w has not undergone chemical exchange, and has only experienced structural dynamics-induced spectral diffusion. In contrast, the other ensemble has undergone chemical exchange. If this ensemble has undergone a single or odd number of exchanges at T_w, it does not contribute to the diagonal peak and does not affect the CLS. However, if there has been two exchanges, that is the population has left and returned to the diagonal peak, or any even number of exchanges, this population will contribute to the diagonal peak and contribute to the CLS at each T_w and to the overall CLS(T_w) decay. When a probe molecule leaves the diagonal band by switching partners from the CN being bound to water to being bound to Li^+ and then switches back to water, it will have a random position in the W inhomogeneous line. That is, an even number of chemical exchange events will contribute a population to the diagonal peak with a CLS of zero (complete loss of frequency correlation).[44] Therefore, the CLS(T_w) decay has two components, one corresponding to structural spectral diffusion (SSD) and the other induced by chemical exchange. We have previously reported the chemical exchange dynamics for the MeSCN/LiCl solutions studied here.[36] Using the known time dependence of the chemical exchange, it is straightforward to remove the chemical exchange contribution to the CLS and obtain the SSD.

At a given T_w, the CLS for a particular diagonal peak is the value it would have if only SSD occurred times the fraction that has not undergone an even number of exchanges plus the CLS after an even number of exchanges (zero) times the fraction that has undergone an even number of exchanges.

$$\mathrm{CLS}_{T_w}^{\mathrm{Exp}} = x_{T_w}^{\mathrm{SSD}}\mathrm{CLS}_{T_w}^{\mathrm{SSD}} + x_{T_w}^{\mathrm{EX}}\mathrm{CLS}_{T_w}^{\mathrm{EX}} = x_{T_w}^{\mathrm{SSD}}\mathrm{CLS}_{T_w}^{\mathrm{SSD}}$$
$$x_{T_w}^{\mathrm{SSD}} + x_{T_w}^{\mathrm{EX}} = 1 \quad (3)$$

Here, the superscripts Exp, SSD, and EX refer to the experiment, structural spectral diffusion, and exchange spectral diffusion. x is the fraction. Because $\mathrm{CLS}_{T_w}^{\mathrm{EX}} = 0$ at all T_w, then

$$\mathrm{CLS}_{T_w}^{\mathrm{SSD}} = \mathrm{CLS}_{T_w}^{\mathrm{Exp}}/x_{T_w}^{\mathrm{SSD}} \quad (4)$$

DOI: 10.1021/acs.jpcb.9b06038
J. Phys. Chem. B XXXX, XXX, XXX−XXX

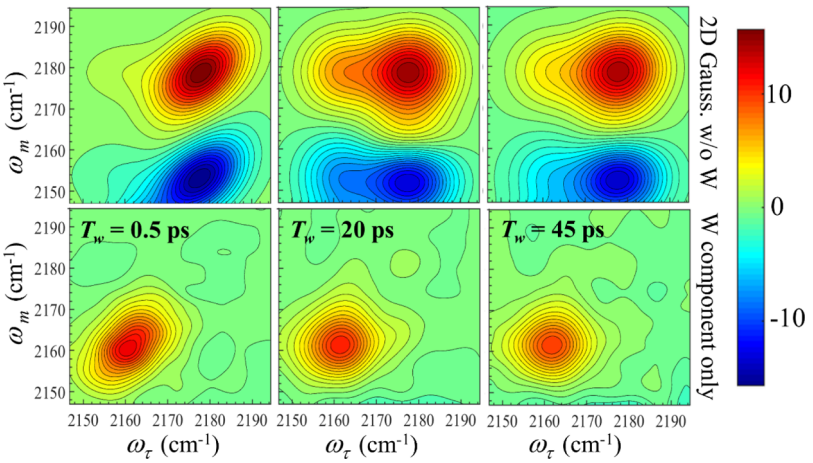

Figure 4. Top panels show 2D reproductions of experimental data with the 2D Gaussian for the W species band omitted at three T_ws (0.5, 20, and 45 ps). The bottom panels show the results of subtracting the top panels from the experimental data. The results are only the W species bands at the three T_ws with all other bands removed. The W bands in the bottom panels are the experimental data, not reproductions.

The desired spectral diffusion dynamics, CLS(T_w), is obtained from the experimental CLS at each T_w and the measured chemical exchange dynamics.[36]

To obtain $x^{SSD}_{T_w}$, one needs to use the experimental chemical exchange results[36] and the kinetic model that describes the exchange. Consider the W diagonal band. In the kinetic model, to get N^S_W, the population of molecules that have stayed (never left) in the original state W, it is only necessary to set k_{LW} (the conversion rate from L to W state) to 0, so that there will be no molecules undergoing multiple exchanges returning molecules to the W diagonal peak.

$$N^S_{T_w} = N_{T_w}(k_{LW} = 0) \tag{5}$$

$$x^{SSD}_{T_w} = N^S_{T_w}/N_{T_w} \tag{6}$$

N_{T_w} is the experimental population of the W diagonal peak, which is proportional to the peak volume. $N^S_{T_w}$ is the population that stayed in the peak, that is, the population it would have without chemical exchange returning population to the diagonal peak. The same type of calculation is performed for the L diagonal peak. Therefore, after isolating the each diagonal peak following the procedure described in section A, the CLS(T_w) that only describes the SSD can be obtained. For the systems studied here, the chemical exchange contribution to the CLS is relatively small. The exchange times L → W and W → L for the three concentrations fall in the ranges of ∼50 and ∼100 ps.[36] The exchange contribution to the CLS requires at least 2 exchanges, away and back, so the time scale is ∼150 ps, which, as discussed below, is long compared to the slowest SSD time scales. The method of elimination of the exchange contribution to recover the SSD is shown to be very accurate in the Supporting Information. Note that in the original detailed chemical exchange theory paper by Kwak et al.,[44] the description of this part of recovering the SSD was confusing; the current presentation is correct.

2.3. Orientational Dynamics. The orientation dynamics of the probe molecules reflects their interactions with surrounding liquid and can shed light on the structural dynamics of the medium. Usually, this dynamical information is extracted via polarization-selective pump−probe (PSPP) experiments as the anisotropy decay. Two probe polarizations, parallel (∥) and perpendicular (⊥), are generally used in this technique. For parallel, the pump and probe pulses have the same polarization, while for perpendicular the probe polarization is perpendicular to the pump. For a single component, the pump−probe signals, $S_\parallel(t)$ and $S_\perp(t)$, can be used to obtain the vibrational relaxation $P(t)$ and the second Legendre polynomial orientational correlation function, $C_2(t)$.[45]

$$S_\parallel(t) = P(t)(1 + 0.8C_2(t))$$
$$S_\perp(t) = P(t)(1 - 0.4C_2(t)) \tag{7}$$

The orientation correlation function is obtained from the anisotropy $r(t)$ by

$$r(t) = \frac{S_\parallel(t) - S_\perp(t)}{S_\parallel(t) + 2S_\perp(t)} = 0.4C_2(t) \tag{8}$$

and the population relaxation is given by

$$P(t) = \frac{1}{3}(S_\parallel(t) + 2S_\perp(t)) \tag{9}$$

In the current system with two species, W and L, and chemical exchange, extraction of the anisotropy becomes more complicated. This is because the two species involved in chemical exchange generally have different reorientation dynamics. The contributions of the two different orientational dynamics are T_w-dependent because of the interconversion between the two species, which means eq 8 no longer holds. The overlap of the 1−2 transition regions further exacerbates the problem. 2D spectra provide a clearer picture. The pump−probe signal at a given time delay t is the projection of the 2D spectrum for $T_w = t$ onto the ω_m axis (see Figure 2). For example, the projection at ω_m = 2179 cm^{-1} in Figure 2 initially reports only on the reorientation of the L component. However, as t increases, the growing cross-peak causes the reorientation dynamics of W component to contribute to the anisotropy.[13,44] The projection at ω_m = 2162 cm^{-1} further involves the 1−2 transition. Therefore, extracting the anisotropy using the PSPP method cannot yield the pure reorientation dynamics of the L or W components.

In our previous publication,[36] the reorientation dynamics of the water-associated and Li^+-associated species were extracted approximately by assuming that the orientation correlation

DOI: 10.1021/acs.jpcb.9b06038
J. Phys. Chem. B XXXX, XXX, XXX−XXX

function is of the form $C_2(t) = \exp(-t/\tau_D)$, where τ_D is a reorientation time constant. However, previous anisotropy measurements of MeSCN in pure water[36] and other molecules containing a CN stretch[46,47] observed biexponential decays, with the fast component analyzed with the wobbling-in-a-cone model.[45,48−51] Therefore, a more rigorous data analysis method is needed.

Figure 2 displays isotropic spectra, that is, they were obtained by measuring the 2D spectra with the polarizations of the first two pulses the same as those of the third pulse and the echo [parallel, $S_{\parallel}^{2D}(T_w)$] and with the first two pulses with polarization perpendicular to the third pulse and the echo (perpendicular, $S_{\perp}^{2D}(T_w)$).[36] Then, the isotropic spectra were obtained as $S_{iso}^{2D}(T_w) = S_{\parallel}^{2D}(T_w) + 2S_{\perp}^{2D}(T_w)$. The 2D spectra obtained in parallel and perpendicular configurations can be processed in the same way as described in connection with Figures 3 and 4. Once isolated diagonal peaks are obtained for each T_w, their projections onto the ω_m axis, namely, the integral along ω_τ of the spectrum for a strip that contains the diagonal peak, can be treated as $S_{\parallel}(t)$ or $S_{\perp}(t)$ depending on the polarization setting of 2D spectra. Thus, within a certain T_w limit, eqs 8 and 9 can be applied to extract the vibrational relaxation and orientational correlation function of a single component without having to remove the effects of chemical exchange mixing the orientational relaxation times of the two species. The T_w limit of this method is determined by the interconversion rate between the W and L species. As explained in Section 2.2, chemical exchange means that even in the isolated diagonal peaks, there are molecules that have undergone even number of exchanges. In the isotropic 2D spectra, the influence of orientational relaxation is eliminated. However, for the $S_{\parallel}^{2D}(T_w)$ and $S_{\perp}^{2D}(T_w)$ spectra, an even number of chemical exchange events will mix in the orientational relaxation of one species with the other. This percentage is defined by $x_{T_w}^{EX}$ in eq 3. Based on the published value of the chemical exchange,[36] $x_{T_w}^{EX}$ is <10% up to T_w = ∼35 ps for the W and L components of all three LiCl solutions. We used this as an empirical boundary where we stopped fitting the anisotropy. We have also fit up to 30 and 40 ps. The change in the time limit had a negligible effect on the fitting results. This method should also be helpful for systems without chemical exchange but with small anharmonicities that lead to overlap between 0−1 and 1−2 signals. For example, in the current system, even without chemical exchange, directly extracting anisotropy of the W component is difficult because the 1−2 transition of L component overlaps with the 0−1 transition of W component. More discussion of this method is included in the Supporting Information.

Figure 5 shows the anisotropy decays for W (top) and L (bottom). The points are the experimental data and the solid curves are the fits. For the W components, the data are fitted with biexponential decays while the anisotropies of L components can be reproduced by single exponential decays. For the W component, the slow decay is the complete orientational relaxation. The faster component is a result of wobbling-in-a-cone.[45,48−51] The orientation samples a limited range of angles, the cone, on a faster time scale followed by constraint release that allows complete orientational randomization. τ_{wob} is the time constant for wobbling in the cone. τ_D is the time constant for complete orientational randomization. The orientational relaxation parameters are given in Table 1. As the LiCl concentration increases, the complete reorientation randomization time constant, τ_D, increases as the viscosity increases. The W τ_D can be compared directly to its value in pure water. The values in the concentrated LiCl solutions scale almost exactly with viscosity from the pure water value (see Table 1). The L values cannot be compared to pure water, but they almost scale with viscosity within the error bars.

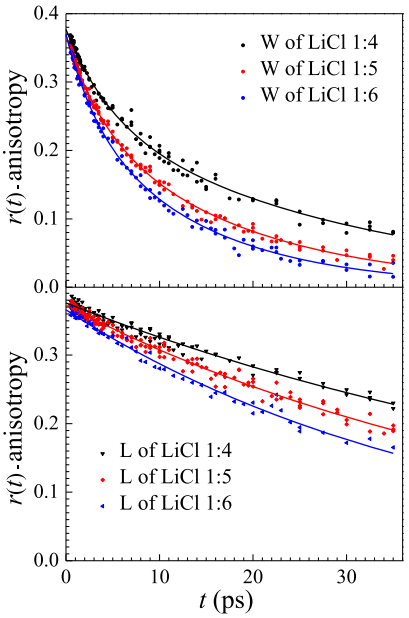

Figure 5. Anisotropy decays of the W species band (top panel) and the L species band (bottom panel) for the three concentrations. The data are obtained from polarized 2D spectra. The interference from the other bands has been removed using the 2D reproduction method described in the text.

Table 1. Summary of Parameters Describing Orientational Relaxation[a,b]

sample	τ_{wob} (ps)	τ_D (ps)	C_1 (ps)	dynamic viscosity (cP)
1:4-W	5.6 ± 0.6	29 ± 3	87 ± 9	6.29 ± 0.06
1:5-W	5.0 ± 0.6	17 ± 2	51 ± 6	4.09 ± 0.06
1:6-W	4.3 ± 0.6	14 ± 2	42 ± 6	3.11 ± 0.05
1:4-L		70 ± 2	210 ± 6	6.29 ± 0.06
1:5-L		52 ± 2	156 ± 6	4.09 ± 0.06
1:6-L		41 ± 2	123 ± 6	3.11 ± 0.05
pure water	1.6 ± 0.3	4.6 ± 0.2		0.90

[a] τ_{wob} and τ_D stand for the time constants for wobbling-in-a-cone component and complete orientation randomization process, respectively. Dynamic viscosities of three LiCl solutions are measured with Ubbelohde viscometer. The dynamic viscosity of pure water is obtained from literature.[67] [b] C_1 is the first Legendre polynomial orientational relaxation decay time constant equal to $3\tau_D$.

The complete orientational relaxation of W at the three LiCl concentrations is much faster than it is for L. These results indicate that the Li^+ bound to the N of the MeSCN likely has a different ion environment than a neutral water bound to the N of the MeSCN. The results suggest that orientational motion of L has higher friction as its reorientation can require concerted motions of the surrounding ion cloud, that is, there are greater electrostatic restraints on L than on W, a neutral species. The same considerations may also explain why W has a wobbling component of the orientation relaxation while L does not. The strong electrostatic interactions of L with the

DOI: 10.1021/acs.jpcb.9b06038
J. Phys. Chem. B XXXX, XXX, XXX−XXX

surrounding ion cloud inhibits small angular wobbling occurring on a time scale that is fast compared to the motion of the surrounding ions.

2.4. Water and Ion Dynamics Characterized by Spectral Diffusion. As discussed above, 2D spectra in the parallel and perpendicular configurations were combined to give $S_{iso}^{2D}(T_w) = S_{\parallel}^{2D}(T_w) + 2S_{\perp}^{2D}(T_w)$.[44] After applying the method described in Sections 2.1 and 2.2 on isotropic 2D spectra, we have extracted the CLS(T_w)s that characterize the SSD only. The CLS(T_w) of the W and L components at three concentrations are plotted in Figure 6A,B (symbols),

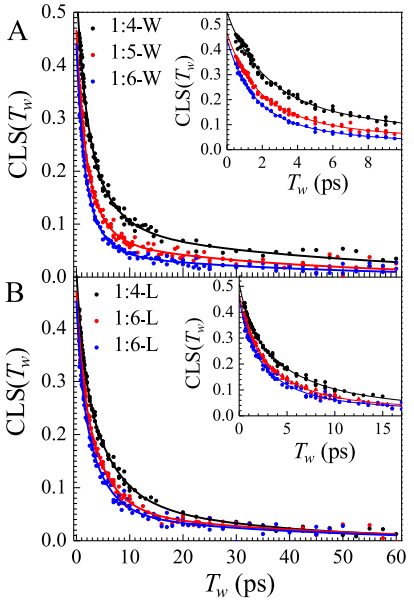

Figure 6. CLS(T_w) decays (points) that characterizes only the SSD. (A,B) are for the W species and L species bands, respectively for three LiCl concentrations. The solid curves are tri-exponential fits to the data. The insets show the short time portions of the data and fits.

respectively. The importance of the method used to obtain the data in Figure 6A,B in comparison to obtaining the CLS(T_w) without removing the effects of interfering bands is discussed in the Supporting Information. The CLS decays of W and L components in Figure 6 were fit with triexponential functions (solid curves). The corresponding FFCF parameters are given in Table 2. For comparison, the FFCF parameters for the CN stretch of MeSCN in pure water are also given.[36]

To understand the timescales of the spectral diffusion in the concentrated LiCl solutions, it is useful to compare the results with the spectral diffusion of the CN stretch of MeSCN in pure water. In pure water using the OD stretch of HOD as the vibrational probe, the spectral diffusion decays as a biexponential with time constants 0.4 ± 0.1 and 1.7 ± 0.1 ps.[52] Simulations have shown that the two time scales, correspond to very local hydrogen bond fluctuations, mainly the length of the H-bond, and the complete randomization of the H-bond network, respectively.[52] Experiments on MeSCN in pure water give the identical time constants.[36] Therefore, it is reasonable to assume the mechanism underlying the spectral diffusion measured with MeSCN in pure water is also H-bond length fluctuations and H-bond network randomization. In contrast to pure water, the FFCFs of both the W and L bands at all concentrations decay as tri-exponential function. It is important to note that the absorption line widths of both the W and L band at all concentrations are ∼1.5 times larger than the bandwidth for pure water (see Table 2, fwhm). There is a small decrease in the fwhm as the concentration is reduced. The L bands are slightly broader than the W bands. The increased width in the LiCl solution has both an increased inhomogeneous and homogenous width. The increase in the inhomogeneous line width is undoubtedly caused by the wide variety of ion configurations that surround the MeSCN probe molecules. Recent experiments and ab initio simulations of concentrated HCl solutions also display two bands in the FT-IR spectrum and in the 2D spectra.[53] The simulations show that one band, the low frequency band, arises when water is H-bounded to the CN nitrogen lone pair, and the other higher-frequency band arises when hydronium is bound to the nitrogen lone pair. The peak with water bound to the N lone pair has virtually the same center frequency as in pure water and as the red peak (W) in the concentrated LiCl spectra. In both the concentrated HCl solutions and in the LiCl solutions, the W peaks are wider than in pure water. The HCl experiments and simulation results are the underpinning for assigning the low-frequency band in LiCl as the W band with water H-bonded to the N lone pair and the higher-frequency band as the L band with Li^+ bound to the N lone pair.

The fastest component, τ_1, of the W FFCF decreases from 1.6 to 1.1 ps, with the values tending toward the pure water value (0.4 ps) as the concentration is reduced (see Table 2). However, this decrease is almost within experimental error. Except for the highest concentration (1:4), the L τ_1 values are the same as the W values within experimental error, and the values for the highest concentration are just outside of error. Previous experiments on other concentrated salt solutions also showed a slow-down of the first spectral diffusion timescale

Table 2. FFCF Parameters That Characterizing Water and Ion Dynamics[b]

sample[a]	Γ (cm^{-1})	Δ_1 (cm^{-1})	τ_1 (ps)	Δ_2 (cm^{-1})	τ_2 (ps)	Δ_3 (cm^{-1})	τ_3 (ps)	fwhm (cm^{-1})
1:4-W	5.0 ± 0.5	4.3 ± 0.4	1.6 ± 0.2	3.3 ± 0.3	4.9 ± 1.0	2.0 ± 0.2	48 ± 12	15.1 ± 0.3
1:5-W	5.2 ± 0.5	4.0 ± 0.4	1.2 ± 0.2	3.4 ± 0.3	3.3 ± 0.6	1.6 ± 0.2	35 ± 10	14.1 ± 0.3
1:6-W	5.1 ± 0.5	4.3 ± 0.4	1.1 ± 0.2	3.1 ± 0.5	3.2 ± 0.5	1.2 ± 0.1	39 ± 10	13.5 ± 0.3
1:4-L	5.6 ± 0.5	4.1 ± 0.4	1.1 ± 0.2	3.9 ± 0.4	5.2 ± 0.8	2.0 ± 0.2	30 ± 7	15.8 ± 0.3
1:5-L	6.0 ± 0.5	3.8 ± 0.4	1.0 ± 0.2	3.9 ± 0.4	4.2 ± 0.8	1.6 ± 0.2	38 ± 7	15.2 ± 0.3
1:6-L	6.1 ± 0.5	3.8 ± 0.4	1.0 ± 0.2	3.7 ± 0.4	3.9 ± 0.8	1.5 ± 0.2	36 ± 7	14.8 ± 0.3
water	3.5 ± 0.3	5.8 ± 1.0	0.4 ± 0.1	2.6 ± 0.2	1.7 ± 0.1			10.5 ± 0.3

[a]Concentrations are labelled as the molar ratio between LiCl and water, such as 1:4. W and L designate the water bound and Li^+ bound to MeSCN diagonal peaks. The row labeled water is the results for MeSCN in pure water. [b]Γ is the homogeneous line width, fwhm of the homogeneous component. Δ_i are the amplitudes (standard deviations) of each component and the τ_i are the corresponding time scales of the FFCF. fwhm (rightmost column) corresponds to the linewidth of experimentally obtained FTIR absorption spectra.

DOI: 10.1021/acs.jpcb.9b06038
J. Phys. Chem. B XXXX, XXX, XXX−XXX

compared to that of pure water.[9,10] In addition, the recent study of MeSCN in concentrated HCl solutions gave a value of τ_1 of 1.1 ps, the same as the values measured here.[53] The τ_2 values for the W and L bands are in the range of ∼5 to ∼3 ps (see Table 2). There is an apparent decrease in the τ_2 values as the concentration is reduced, but the decrease falls within the error bars. The values of τ_1 and τ_2 for both the W and L bands are a factor of 2.5−3 slower than the values in pure water.

We therefore assign the fastest component to local length fluctuation of the N−HO distance when water is bound to the N lone pair (W) and the N−Li^+ distance when Li^+ is bound to the N lone pair. The middle time constant, τ_2, of the W band decreases from 4.9 to 3.2 ps as the LiCl concentration is reduced. Although there are significant error bars, as the concentration is lowered, the time constant approaches the 1.7 ps value measured in pure water.[36,52] It is reasonable to take the middle time constants of both the W and L species as corresponding to the 1.7 ps dynamics in pure water, which represents the global hydrogen bond network reorganization. This trend has been observed previously in less concentrated solutions of a variety of cation/anion pairs,[9] where molar ratio of cation to water ranged from 1:16 to 1:56. Results from a study of an even more concentrated salt solution of lithium bis(trifluoromethane)sulfonimide ($LiNTf_2$) where the ratio is 1:2.5, gave a second time constant of ∼17 ps.[10] In this system, the anion is very large compared to Cl^-.

In pure water, the CLS is a bi-exponential decay with a slowest component of 1.7 ps. The inhomogeneity in pure water is caused solely by the range of H-bond configurations. In the concentrated LiCl solutions, the corresponding component of the tri-exponential CLS decay is the middle component. In the LiCl solutions, the inhomogeneous broadening of the absorption line is significantly broader than in pure water (see Table 2). The configurations of ions in the vicinities of the probes contribute to the inhomogeneous broadening. To completely sample the inhomogeneous line, the ion configurations that contribute to the inhomogeneous broadening have to randomize.

In the LiCl solutions, in which the molar ratio of Li^+ and water is between 1:4 to 1:6, there is not enough water to fully solvate Li^+ and Cl^- individually,[5,54] that is, there are no isolated solvated ions. Water bridges are common between two oppositely charged ions[54] and this undermines the extended water network that facilitates breaking and forming hydrogen bonds and reorientation. The slowing of reorientation of water molecules has been attributed to the strong effect of ion clusters in concentrated salt solutions.[23,24] As the salt concentration increases, the extent of the hydrogen bond network becomes smaller and more localized;[34] thus the concerted randomization process that occurs in pure water becomes more difficult and slower. In addition, hydrogen bond rearrangement alone cannot sample all the liquid structures that give rise to the inhomogeneously broadened absorption spectrum. Therefore, H-bond rearrangement will not produce complete spectral diffusion ($CLS(T_w) \rightarrow 0$).

The slowest component of the spectral diffusion, τ_3 = ∼40 ps for both W and L within experimental error (see Table 2), reflects distinct dynamics in the LiCl solutions that do not exist in pure water. A similar slow component is not observable in lower concentration salt solutions,[9] but is observed in high-concentration studies.[10] As can be seen in Table 2, for the water bound to MeSCN (W), the amplitudes of this component, Δ_3, decrease from 2.0 to 1.2 cm^{-1} and the L component decreases from 2.0 to 1.5 cm^{-1} in going from LiCl 1:4 to 1:6 solutions. As reported in an MD simulation study of LiCl solutions,[55] the percentage of ions in dimer ion pairs increases from ∼25 to 43%, which corresponds nicely to the increase in Δ_3. The large increase of ion pairs or clusters as the concentration increases has also been reported in other publications.[11,55−57] Therefore, we assign the ∼40 ps spectral diffusion dynamics to ion cluster dynamics, or more specifically the restructuring of ion pairs or larger clusters.

The assignment of the slowest component of the spectral diffusion to ion cluster dynamics is supported by both theory and experiment. Many simulations have been conducted to examine ion pair and cluster dynamics. Lipowsky et al. conducted MD simulation of 0.5−3.5 M salt solutions and compared the ion cluster lifetime of cesium chloride (CsCl) and magnesium sulfate ($MgSO_4$).[58] For CsCl, both contact ion pair and solvent-shared ion pair (SIP) lifetimes of 5−7 ps were found. For $MgSO_4$, the SIP lifetimes of 100−200 ps were reported while the solvent-separated ion pairs (2SIP) had lifetimes of 20−50 ps. The difference between the two types of salt solutions largely originates from differences in their viscosities and electrostatic interactions.[58] The LiCl solutions studied here lie between CsCl and $MgSO_4$ in viscosity.[59] LiCl electrostatic interactions should be stronger than CsCl because Li^+ is smaller and thus has a higher charge density. However, the interaction should be weaker than $MgSO_4$ because both Mg^{2+} and SO_4^{2-} ions are doubly charged. Therefore, the LiCl ion pair lifetime is likely between those of CsCl and $MgSO_4$. Note, the MD simulations were performed up to 3.5 M salt solutions; the ion pair lifetimes should be longer in the higher concentrations studied here.[58] Using 2D IR chemical exchange spectroscopy, Bian et al. estimated the exchange time between clustered and isolated thiocyanate anions to be ∼12 ps in concentrated potassium thiocyanate solutions.[11] Park et al. measured perchlorate−thiocyanate anion exchange in the first solvation shell of the Mg^{2+} cation to be ∼50 ps in a concentrated aqueous salt solution.[16]

Therefore, simulations and experiments support the proposition that the ∼40 ps spectral diffusion time constant, τ_3, is the timescale for ion pair and ion cluster dynamics. This slowest component of the spectral diffusion samples all the remaining frequencies and therefore all structures of the liquid as shown by the decay of the $CLS(T_w)$ to zero or virtually to zero on the time scale of the experiments (see Figure 6). If the ion clouds surrounding the vibrational probes structurally relaxed on time scales longer than ∼40 ps, then the $CLS(T_w)$ would not decay to zero. Therefore, 40 ps is the time scale for complete randomization of the ion structures.

All three FFCF time constants for the W and L bands are essentially the same. MeSCN with its bound species, H_2O or Li^+, are embedded in a concentrated sea of ions and water. The CN stretch spectral diffusion reports on the dynamics of its surroundings. The similarity of the W and L time constants indicates that the structure and dynamics of the medium in the vicinity of the probe is not influenced to a significant extent whether an H_2O or Li^+ is bound to the N lone pair. The spectral diffusion, particularly τ_2 and τ_3, reports on dynamics of a significant volume around the probe, reducing the impact of which species is bound to the probe. However, as shown in Table 1 and discussed further below, the species bound to the probe does have a major impact on orientational relaxation.

While the spectral diffusion time constants for the W and L species are basically the same, we did observe a small difference

DOI: 10.1021/acs.jpcb.9b06038
J. Phys. Chem. B XXXX, XXX, XXX−XXX

in the nature of the 2D IR observables depending on which species is bound to the probe. We extracted the CLS(T_w) from 2D spectra with parallel and perpendicular polarizations following the method described in Sections 2.1 and 2.2. Figure 7 displays data for the LiCl 1:5 H_2O solution. Figure 7A

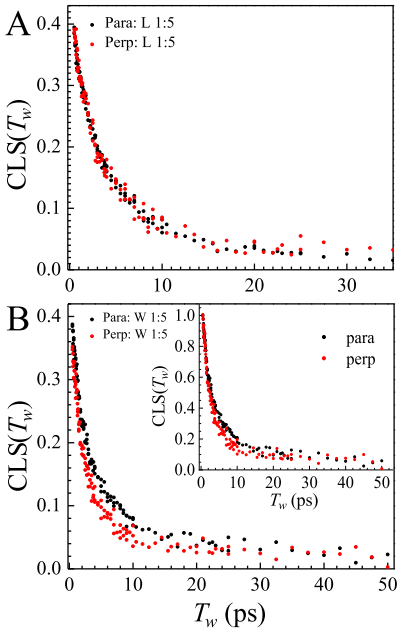

Figure 7. CLS(T_w) decays taken with parallel and perpendicular polarizations. The L species data (A) has no polarization dependence. The W species data (B) has a small polarization dependence. The inset shows the W data normalized at $\sim T_w = 0$. The normalized data shows even less polarization dependence.

shows the data for the L band. The two scans are identical, demonstrating that the CLS(T_w) is independent of polarization. However, the data for the W band shown in Figure 7B has a small polarization dependence as the two curves are not coincident. Much of the difference occurs on a time scale too short for us to resolve as shown by the fact that the parallel curve has somewhat greater amplitude than the perpendicular curve at $T_w = \sim 0$. The inset shows the curves normalized at the shortest time to eliminate the effect of the vertical offset at $T_w = \sim 0$. The difference in the two curves is reduced, but not completely eliminated. The differences in the curves occur at $T_w = \sim 0$ and at intermediate times. Similar differences were also observed in the other two concentration solutions.

The L species parallel and perpendicular polarization CLS(T_w)s (Figure 7A) are identical while the W data (Figure 7B) are not. Orientational relaxation can be responsible for the difference of the W and L data. The W orientation relaxation is a biexponential and the slow component is significantly faster than the single decay of L. The reorientation-induced spectral diffusion (RISD) model[60,61] has previously successfully described large differences in polarization-dependent CLS(T_w)s. For example, carbon dioxide generally has weak interactions with ionic liquids and its polarization-dependent CLS can be explained by this model extremely well.[61] However, the theory fails to describe the small differences in the polarization-dependent CLS(T_w)s shown in Figure 7B. This failure likely originates from the assumption that underpins the RISD theory, that is, the reorientation of probe molecules is independent of the structural evolution of the liquid that causes SSD. For example, water probed with the OD stretch of HOD in H_2O does not display RISD although the slowest component of the spectral diffusion and the orientational relaxation occur on the same time scale. The lack of RISD (a polarization dependence to the CLS(T_w) decays) in water is a result of hydrogen bond rearrangement being responsible for both the spectral diffusion and the orientation relaxation. Here, the W intermediate time scale wobbling in a cone is almost but not quite tied to structural relaxation, resulting in a small polarization difference.

There is another issue that needs to be addressed involving the relationship between the spectral diffusion and the orientational relaxation, particularly for W. In Table 2, the slowest component of the W spectral diffusion is actually slower than the orientational relaxation, τ_D, given in Table 1. For L, τ_D is somewhat slower than the slowest component of the spectral diffusion. The question is how can the spectral diffusion be slower than the orientational relaxation? The slowest component of the SSD, the third exponential, is not present in pure water. This component is assigned to the structural evolution of ion pairs and clusters. The ion configurations will couple to the CN stretch frequency via the first-order Stark effect.[62,63] The first-order vibrational Stark effect involves the coupling of an electric field to the dipole moment difference that arises when the vibration, CN in this case, is excited. As the ion cloud reconfigures, the electric field will change, causing the vibrational frequency to change. The frequency shift is linearly proportional to electric field via the Stark tuning rate.[64,65] Based on the contribution of the ion cloud to the inhomogeneous line width (Δ_3 of the W components in Table 2), the root mean square electric field amplitude (standard deviation for a Gaussian distribution) along the CN bond is ~3.3 MV/cm for the LiCl 1:4 H_2O solution, decreasing to ~2 MV/cm for LiCl 1:6 H_2O solution. These values serve as an observable that can be readily obtained from future simulation studies of concentrated LiCl solutions and are useful to vet the accuracy of the simulations.

Spectral diffusion gives rise to the FFCF. Based on the Stark effect, this function is equivalent to electric-field correlation function, whose appropriate correlation function form is $C_1(t) = \exp(-l(l+1)D_0t) = \exp(-2D_0t)$, the first Legendre polynomial correlation function where $l = 1$ and D_0 is the orientational diffusion coefficient.[60] The PSPP, on the other hand, measures $C_2(t)$, the second Legendre polynomial correlation function, which is second order in the electric field of the light. The exponential decay time constant $\tau_D = 1/6D_\theta$. Therefore, when comparing orientational relaxation times to the spectral diffusion times, the comparison is between τ_3 in Table 2 and C_1 in Table 1. For W, the orientational relaxation is slower or about the same as the slowest component of the spectral diffusion. For L, the orientational relaxation is much slower than the slowest component of the spectral diffusion. Therefore, there is no contradiction between the measured orientational relaxation rates and the slowest components of the spectral diffusion.

The fact that for W, τ_3 and $C_1(t)$ occur on similar time scales (see Tables 1 and 2), suggests that orientational relaxation MeSCN·H_2O occurs because the ion cloud, that is, ion pairs, ion clusters, and so forth, structurally rearranges. The same structural rearrangements cause the electric field along the CN bond to evolve in time, giving rise to the slowest component of the spectral diffusion via the first-order Stark effect. The τ_3 values for W and L are equivalent within experimental error

DOI: 10.1021/acs.jpcb.9b06038
J. Phys. Chem. B XXXX, XXX, XXX−XXX

(see Table 2). The same τ_3 time constants for W and L indicate that the mechanism is the same for the slowest component of the spectral diffusion reported by the CN stretch. However, the relevant orientational relaxation times, C_1, are much slower for L than for W. These results suggest that the neutral species MeSCN·H_2O can undergo orientational relaxation with structural changes in the ion cloud that are insufficient to enable the charged species MeSCN·Li^+ to change its orientation to the same extent. For example, MeSCN·Li^+ may be tightly pinned to an adjacent Cl^- while the water on MeSCN·H_2O makes relative weak H-bonds to Cl^-.[19,66] Restructuring of the ion cloud nearby, which contributes to spectral diffusion, may allow MeSCN·H_2O to take an angular step by breaking its H-bond to the still adjacent Cl^- while the strong interaction of MeSCN·Li^+ and an adjacent Cl^- prevents a similar step from occurring. The result of this scenario is that W and L have the same spectral diffusion time constants within error, but W has substantially faster orientational relaxation.

3. CONCLUDING REMARKS

We employed the CN stretch of MeSCN as the vibrational probe to interrogate ion dynamics in concentrated LiCl aqueous solutions as a function of concentration. MeSCN has two absorption peaks in the LiCl solutions, one corresponding to water-associated (W) and the other corresponding to Li^+-associated (L) with the nitrogen lone pair of MeSCN. Using polarization-selective 2D IR spectroscopy, we have measured spectral diffusion, which reports on the structural dynamics of the solutions and orientational relaxation of the W and L species. Spectral diffusion is caused by the solution dynamics as reported by the probe.

Because of the small separation of the two overlapping absorption bands, chemical exchange events, which produce time-dependent off-diagonal peaks,[36] and the 1−2 transition off-diagonal bands, the 2D IR spectra are complex and crowded. To obtain the FFCF from the time-dependent shapes of the diagonal bands required the development of a new method. The normalized FFCF is obtained using the CLS method.[38] By modeling the overlapping peaks as 2D Gaussians and subtracting these 2D Gaussians, the diagonal peak of interest is obtained (see Figure 4). This remaining peak is the experimental data, not a 2D Gaussian replica. With a single diagonal peak, from either W or L, we were able to accurately obtain the CLS(T_w) data. It is important to note, that depending on the 2D band shapes, functional forms other than 2D Gaussians may appropriate.

The CLS(T_w) of the isolated peak is dominated by SSD, (structural evolution of the liquid) but it has a small contribution from chemical exchange-induced spectral diffusion. We presented a method to remove the chemical exchange contribution and obtained the pure SSD.

In contrast to the 2D IR experiments on pure water, which display a biexponential decay of the FFCF, the SSD in the concentrated LiCl solutions decays as a tri-exponential. The two faster components are ∼3 times slower than the corresponding decays in pure water (see Table 2). In analogy to pure water, we assign the fastest component to very local positon fluctuations of the species, water or Li^+, which is bound to the nitrogen lone pair of the CN. The second component of the tri-exponential FFCF reflects H-bond rearrangement. The high concentration of LiCl results in broader inhomogeneous lines than the line width of the CN stretch in pure water. The third slowest component of the FFCF is associated with randomization of the ion cloud, that is, ion pairs, water-separated ion pairs, and ion clusters. The ion cloud can influence the frequency of the CN stretch via the first-order Stark effect. Randomization of the ion cloud is necessary to sample the extra inhomogeneous width of the absorption line. The time scale of the slowest SSD component is ∼40 ps, which is the time for randomization of the ion cloud structure to the extent that all configurations that contribute to the inhomogeneous CN frequency distribution have been sampled.

Because of the interfering off-diagonal chemical exchange and 1−2 transition peaks, it is complicated to obtain the orientational relaxation via the standard polarization-selective pump−probe experiment. Instead, we employed polarization-selective 2D IR experiments. The same method as used to obtain an isolated diagonal peak for the determination of the FFCF was employed to obtain the anisotropy. However, rather than performing the CLS analysis on the isolated peak, it was integrated along the ω_τ axis (horizontal axis) projecting it onto the ω_m axis (vertical axis) for each polarization at each time. This projection gives the equivalent of the pump−probe anisotropy measurements, but with the interfering peaks removed. It was found that MeSCN·Li^+ undergoes orientational relaxation much slower than MeSCN·H_2O, likely because of strong electrostatic interactions of the charged species compared to the weaker interactions of the neutral species. The relationships between the time scales of SSD and orientational relaxation were also considered.

The results that emerge present a detailed view of dynamics and interactions in concentrated aqueous ionic solutions. In addition, two new methods were presented. One enables accurate determination of the FFCF in spite of crowded 2D IR spectra with overlapping time-dependent peaks. This method should also be applicable in 2D electronic excited-state spectroscopy. The second method makes it possible to extract orientational relaxation using polarized 2D IR spectroscopy again by removing the influences of overlapping bands.

■ ASSOCIATED CONTENT

Supporting Information

The Supporting Information is available free of charge on the ACS Publications website at DOI: 10.1021/acs.jpcb.9b06038.

Band shape analysis method; validation of anisotropy extracting method; and simulation validation of chemical exchange-induced spectral diffusion (PDF)

■ AUTHOR INFORMATION

Corresponding Author

*E-mail: fayer@stanford.edu. Phone: 650 723-4446.

ORCID

Rongfeng Yuan: 0000-0002-6572-2472

Michael D. Fayer: 0000-0002-0021-1815

Notes

The authors declare no competing financial interest.

■ ACKNOWLEDGMENTS

We would like to thank Steven Yamada and Dr. Qian Lin for helpful discussions of chemical exchange induced spectral diffusion. We would like to thank Sean Roget for discussions of the development of the 2D Subtraction method. This work was

supported in part by the Division of Chemical Sciences, Geosciences, and Biosciences, Office of Basic Energy Sciences of the U.S. Department of Energy through grant no. DEFG03-84ER13251 (R.Y., MDF), and in part by the Air Force Office of Scientific Research under AFOSR award no. FA9550-16-1-0104 (MDF and the ultrafast IR spectrometer).

REFERENCES

(1) Marcus, Y. Effect of Ions on the Structure of Water: Structure Making and Breaking. *Chem. Rev.* **2009**, *109*, 1346−1370.
(2) Mamontov, E.; De Francesco, A.; Formisano, F.; Laloni, A.; Sani, L.; Leu, B. M.; Said, A. H.; Kolesnikov, A. I. Water Dynamics in a Lithium Chloride Aqueous Solution Probed by Brillouin Neutron and X-Ray Scattering. *J. Phys.: Condens. Matter* **2012**, *24*, 064102.
(3) Terpstra, P.; Combes, D.; Zwick, A. Effect of Salts on Dynamics of Water - a Raman-Spectroscopy Study. *J. Chem. Phys.* **1990**, *92*, 65−70.
(4) Bajaj, P.; Richardson, J. O.; Paesani, F. Ion-Mediated Hydrogen-Bond Rearrangement through Tunnelling in the Iodide-Dihydrate Complex. *Nat. Chem.* **2019**, *11*, 367−374.
(5) Harsányi, I.; Pusztai, L. Hydration Structure in Concentrated Aqueous Lithium Chloride Solutions: A Reverse Monte Carlo Based Combination of Molecular Dynamics Simulations and Diffraction Data. *J. Chem. Phys.* **2012**, *137*, 204503.
(6) Cota, R.; Ottosson, N.; Bakker, H. J.; Woutersen, S. Evidence for Reduced Hydrogen-Bond Cooperativity in Ionic Solvation Shells from Isotope-Dependent Dielectric Relaxation. *Phys. Rev. Lett.* **2018**, *120*, 216001.
(7) Chizhik, B. V. I. NMR Relaxation and Microstructure of Aqueous Electrolyte Solutions. *Mol. Phys.* **1997**, *90*, 653−659.
(8) Akitt, J. W. Multinuclear Nuclear Magnetic-Resonance Studies of Aqueous-Solutions of Tetrafluoroborate Salts. *J. Chem. Soc., Faraday Trans. 1* **1975**, *71*, 1557.
(9) Giammanco, C. H.; Wong, D. B.; Fayer, M. D. Water Dynamics in Divalent and Monovalent Concentrated Salt Solutions. *J. Phys. Chem. B* **2012**, *116*, 13781−13792.
(10) Giammanco, C. H.; Kramer, P. L.; Fayer, M. D. Ionic Liquid Versus Li^+ Aqueous Solutions: Water Dynamics near Bistriflimide Anions. *J. Phys. Chem. B* **2016**, *120*, 9997−10009.
(11) Bian, H.; Wen, X.; Li, J.; Chen, H.; Han, S.; Sun, X.; Song, J.; Zhuang, W.; Zheng, J. Ion Clustering in Aqueous Solutions Probed with Vibrational Energy Transfer. *Proc. Natl. Acad. Sci. U.S.A.* **2011**, *108*, 4737−4742.
(12) Tielrooij, K. J.; Garcia-Araez, N.; Bonn, M.; Bakker, H. J. Cooperativity in Ion Hydration. *Science* **2010**, *328*, 1006−1009.
(13) Ji, M.; Odelius, M.; Gaffney, K. J. Large Angular Jump Mechanism Observed for Hydrogen Bond Exchange in Aqueous Perchlorate Solution. *Science* **2010**, *328*, 1003−1005.
(14) Moilanen, D. E.; Wong, D.; Rosenfeld, D. E.; Fenn, E. E.; Fayer, M. D. Ion-Water Hydrogen-Bond Switching Observed with 2D IR Vibrational Echo Chemical Exchange Spectroscopy. *Proc. Natl. Acad. Sci. U.S.A.* **2009**, *106*, 375−380.
(15) Sun, Z.; Zhang, W.; Ji, M.; Hartsock, R.; Gaffney, K. J. Contact Ion Pair Formation between Hard Acids and Soft Bases in Aqueous Solutions Observed with 2D IR Spectroscopy. *J. Phys. Chem. B* **2013**, *117*, 15306−15312.
(16) Park, S.; Ji, M.; Gaffney, K. J. Ligand Exchange Dynamics in Aqueous Solution Studied with 2DIR Spectroscopy. *J. Phys. Chem. B* **2010**, *114*, 6693−6702.
(17) Ji, M.; Hartsock, R. W.; Sun, Z.; Gaffney, K. J. Interdependence of Conformational and Chemical Reaction Dynamics During Ion Assembly in Polar Solvents. *J. Phys. Chem. B* **2011**, *115*, 11399−11408.
(18) Kropman, M. F.; Bakker, H. J. Dynamics of Water Molecules in Aqueous Solvation Shells. *Science* **2001**, *291*, 2118−2120.
(19) Smith, J. D.; Saykally, R. J.; Geissler, P. L. The Effect of Dissolved Halide Anions on Hydrogen Bonding in Liquid Water. *J. Am. Chem. Soc.* **2007**, *129*, 13847−13856.
(20) Lin, Y.-S.; Auer, B. M.; Skinner, J. L. Water Structure, Dynamics, and Vibrational Spectroscopy in Sodium Bromide Solutions. *J. Chem. Phys.* **2009**, *131*, 144511.
(21) Suo, L.; Borodin, O.; Gao, T.; Olguin, M.; Ho, J.; Fan, X.; Luo, C.; Wang, C.; Xu, K. "Water-in-salt" electrolyte enables high-voltage aqueous lithium-ion chemistries. *Science* **2015**, *350*, 938−943.
(22) Cheng, X.-B.; Zhang, R.; Zhao, C.-Z.; Zhang, Q. Toward Safe Lithium Metal Anode in Rechargeable Batteries: A Review. *Chem. Rev.* **2017**, *117*, 10403−10473.
(23) Stirnemann, G.; Wernersson, E.; Jungwirth, P.; Laage, D. Mechanisms of Acceleration and Retardation of Water Dynamics by Ions. *J. Am. Chem. Soc.* **2013**, *135*, 11824−11831.
(24) Zhang, Q.; Wu, T.; Chen, C.; Mukamel, S.; Zhuang, W. Molecular Mechanism of Water Reorientational Slowing Down in Concentrated Ionic Solutions. *Proc. Natl. Acad. Sci. U.S.A.* **2017**, *114*, 10023−10028.
(25) Han, S. Dynamic Features of Water Molecules in Super-concentrated Aqueous Electrolytes. *Sci. Rep.* **2018**, *8*, 9347.
(26) Jungwirth, P.; Cremer, P. S. Beyond Hofmeister. *Nat. Chem.* **2014**, *6*, 261−263.
(27) Xie, W. J.; Gao, Y. Q. A Simple Theory for the Hofmeister Series. *J. Phys. Chem. Lett.* **2013**, *4*, 4247−4252.
(28) Aragones, J. L.; Rovere, M.; Vega, C.; Gallo, P. Computer Simulation Study of the Structure of LiCl Aqueous Solutions: Test of Non-Standard Mixing Rules in the Ion Interaction. *J. Phys. Chem. B* **2014**, *118*, 7680−7691.
(29) Santucci, S. C.; Comez, L.; Scarponi, F.; Monaco, G.; Verbeni, R.; Legrand, J.-F.; Masciovecchio, C.; Gessini, A.; Fioretto, D. Onset of the Alpha-Relaxation in the Glass-Forming Solution LiCl-$6H_2O$ Revealed by Brillouin Scattering Techniques. *J. Chem. Phys.* **2009**, *131*, 154507.
(30) Ibuki, K.; Bopp, P. A. Molecular Dynamics Simulations of Aqueous LiCl Solutions at Room Temperature through the Entire Concentration Range. *J. Mol. Liq.* **2009**, *147*, 56−63.
(31) Harsányi, I.; Temleitner, L.; Beuneu, B.; Pusztai, L. Neutron and X-Ray Diffraction Measurements on Highly Concentrated Aqueous LiCl Solutions. *J. Mol. Liq.* **2012**, *165*, 94−100.
(32) Lee, K.-K.; Park, K.-H.; Kwon, D.; Choi, J.-H.; Son, H.; Park, S.; Cho, M. Ion-Pairing Dynamics of Li^+ and SCN^- in Dimethylformamide Solution: Chemical Exchange Two-Dimensional Infrared Spectroscopy. *J. Chem. Phys.* **2011**, *134*, 064506.
(33) Pluhařová, E.; Mason, P. E.; Jungwirth, P. Ion Pairing in Aqueous Lithium Salt Solutions with Monovalent and Divalent Counter-Anions. *J. Phys. Chem. A* **2013**, *117*, 11766−11773.
(34) Juurinen, I.; Pylkkänen, T.; Ruotsalainen, K. O.; Sahle, C. J.; Monaco, G.; Hämäläinen, K.; Huotari, S.; Hakala, M. Saturation Behavior in X-Ray Raman Scattering Spectra of Aqueous LiCl. *J. Phys. Chem. B* **2013**, *117*, 16506−16511.
(35) Corridoni, T.; Mancinelli, R.; Ricci, M. A.; Bruni, F. Viscosity of Aqueous Solutions and Local Microscopic Structure. *J. Phys. Chem. B* **2011**, *115*, 14008−14013.
(36) Yuan, R.; Yan, C.; Fayer, M. Ion-Molecule Complex Dissociation and Formation Dynamics in LiCl Aqueous Solutions from 2D IR Spectroscopy. *J. Phys. Chem. B* **2018**, *122*, 10582−10592.
(37) Kwak, K.; Park, S.; Finkelstein, I. J.; Fayer, M. D. Frequency-Frequency Correlation Functions and Apodization in Two-Dimensional Infrared Vibrational Echo Spectroscopy: A New Approach. *J. Chem. Phys.* **2007**, *127*, 124503.
(38) Kwak, K.; Rosenfeld, D. E.; Fayer, M. D. Taking Apart the Two-Dimensional Infrared Vibrational Echo Spectra: More Information and Elimination of Distortions. *J. Chem. Phys.* **2008**, *128*, 204505.
(39) Kubo, R. *Fluctuation, Relaxation, and Resonance in Magnetic Systems*; Haar, D. T., Ed.; Oliver and Boyd: London, 1962; Vol. *viii*, p 320.
(40) Hamm, P.; Zanni, M. T. *Concepts and Methods of 2D Infrared Spectroscopy*; Cambridge University Press: Cambridge, New York, 2011.

DOI: 10.1021/acs.jpcb.9b06038
J. Phys. Chem. B XXXX, XXX, XXX−XXX

(41) Giammanco, C. H.; Kramer, P. L.; Fayer, M. D. Dynamics of Dihydrogen Bonding in Aqueous Solutions of Sodium Borohydride. *J. Phys. Chem. B* **2015**, *119*, 3546−3559.
(42) Fenn, E. E.; Fayer, M. D. Extracting 2D IR Frequency-Frequency Correlation Functions from Two Component Systems. *J. Chem. Phys.* **2011**, *135*, 07450.
(43) Rubtsov, I. V.; Wang, J.; Hochstrasser, R. M. Dual Frequency 2D-IR of Peptide Amide-a and Amide-I Modes. *J. Chem. Phys.* **2003**, *118*, 7733−7736.
(44) Kwak, K.; Zheng, J.; Cang, H.; Fayer, M. D. Ultrafast 2D IR Vibrational Echo Chemical Exchange Experiments and Theory. *J. Phys. Chem. B* **2006**, *110*, 19998−20013.
(45) Tan, H.-S.; Piletic, I. R.; Fayer, M. D. Orientational Dynamics of Water Confined on a Nanometer Length Scale in Reverse Micelles. *J. Chem. Phys.* **2005**, *122*, 174501.
(46) Yuan, R.; Yan, C.; Tamimi, A.; Fayer, M. D. Molecular Anion Hydrogen Bonding Dynamics in Aqueous Solution. *J. Phys. Chem. B* **2015**, *119*, 13407−13415.
(47) Yamada, S. A.; Thompson, W. H.; Fayer, M. D. Water-Anion Hydrogen Bonding Dynamics: Ultrafast IR Experiments and Simulations. *J. Chem. Phys.* **2017**, *146*, 234501.
(48) Kinosita, K., Jr.; Kawato, S.; Ikegami, A. A Theory of Fluorescence Polarization Decay in Membranes. *Biophys. J.* **1977**, *20*, 289−305.
(49) Lipari, G.; Szabo, A. Effect of Librational Motion on Fluorescence Depolarization and Nuclear Magnetic-Resonance Relaxation in Macromolecules and Membranes. *Biophys. J.* **1980**, *30*, 489−506.
(50) Lipari, G.; Szabo, A. Model-Free Approach to the Interpretation of Nuclear Magnetic-Resonance Relaxation in Macromolecules .1. Theory and Range of Validity. *J. Am. Chem. Soc.* **1982**, *104*, 4546−4559.
(51) Wang, C. C.; Pecora, R. Time-Correlation Functions for Restricted Rotational Diffusion. *J. Chem. Phys.* **1980**, *72*, 5333−5340.
(52) Asbury, J. B.; Steinel, T.; Kwak, K.; Corcelli, S. A.; Lawrence, C. P.; Skinner, J. L.; Fayer, M. D. Dynamics of Water Probed with Vibrational Echo Correlation Spectroscopy. *J. Chem. Phys.* **2004**, *121*, 12431.
(53) Yuan, R.; Napoli, J. A.; Yan, C.; Marsalek, O.; Markland, T. E.; Fayer, M. D. Tracking Aqueous Proton Transfer by Two-Dimensional Infrared Spectroscopy and Ab Initio Molecular Dynamics Simulations. *ACS Cent. Sci.* **2019**, *5*, 1269−1277.
(54) Petit, L.; Vuilleumier, R.; Maldivi, P.; Adamo, C. Ab Initio Molecular Dynamics Study of a Highly Concentrated LiCl Aqueous Solution. *J. Chem. Theory Comput.* **2008**, *4*, 1040−1048.
(55) Singh, M. B.; Dalvi, V. H.; Gaikar, V. G. Investigations of Clustering of Ions and Diffusivity in Concentrated Aqueous Solutions of Lithium Chloride by Molecular Dynamic Simulations. *RSC Adv.* **2015**, *5*, 15328−15337.
(56) Fennell, C. J.; Bizjak, A.; Vlachy, V.; Dill, K. A. Ion Pairing in Molecular Simulations of Aqueous Alkali Halide Solutions. *J. Phys. Chem. B* **2009**, *113*, 6782−6791.
(57) Bouazizi, S.; Nasr, S. Local Order in Aqueous Lithium Chloride Solutions as Studied by X-Ray Scattering and Molecular Dynamics Simulations. *J. Mol. Struct.* **2007**, *837*, 206−213.
(58) Verde, A. V.; Santer, M.; Lipowsky, R. Solvent-Shared Pairs of Densely Charged Ions Induce Intense but Short-Range Supra-Additive Slowdown of Water Rotation. *Phys. Chem. Chem. Phys.* **2016**, *18*, 1918−1930.
(59) Concentrative Properties of Aqueous Solutions: Density, Refractive Index, Freezing Point Depression, and Viscosity. In *CRC Handbook of Chemistry and Physics*, 99th ed.; Rumble, J. R., Ed.; CRC Press/Taylor & Francis: Boca Raton, FL, 2018.
(60) Kramer, P. L.; Nishida, J.; Giammanco, C. H.; Tamimi, A.; Fayer, M. D. Observation and Theory of Reorientation-Induced Spectral Diffusion in Polarization-Selective 2D IR Spectroscopy. *J. Chem. Phys.* **2015**, *142*, 184505.
(61) Giammanco, C. H.; Kramer, P. L.; Yamada, S. A.; Nishida, J.; Tamimi, A.; Fayer, M. D. Coupling of Carbon Dioxide Stretch and Bend Vibrations Reveals Thermal Population Dynamics in an Ionic Liquid. *J. Phys. Chem. B* **2016**, *120*, 549−556.
(62) Bagchi, S.; Boxer, S. G.; Fayer, M. D. Ribonuclease S Dynamics Measured Using a Nitrile Label with 2D IR Vibrational Echo Spectroscopy. *J. Phys. Chem. B* **2012**, *116*, 4034−4042.
(63) Williams, R. B.; Loring, R. F.; Fayer, M. D. Vibrational Dephasing of Carbonmonoxy Myoglobin. *J. Phys. Chem. B* **2001**, *105*, 4068−4071.
(64) Andrews, S. S.; Boxer, S. G. Vibrational Stark Effects of Nitriles I. Methods and Experimental Results. *J. Phys. Chem. A* **2000**, *104*, 11853−11863.
(65) Błasiak, B.; Ritchie, A. W.; Webb, L. J.; Cho, M. Vibrational Solvatochromism of Nitrile Infrared Probes: Beyond the Vibrational Stark Dipole Approach. *Phys. Chem. Chem. Phys.* **2016**, *18*, 18094−18111.
(66) Thompson, W. H.; Hynes, J. T. Frequency Shifts in the Hydrogen-Bonded Oh Stretch in Halide-Water Clusters. The Importance of Charge Transfer. *J. Am. Chem. Soc.* **2000**, *122*, 6278−6286.
(67) Crittenden, J. C.; Trussell, R. R.; Hand, D. W.; Howe, K. J.; Tchobanoglous, G. Appendix C Physical Properties of Water. *MWH's Water Treatment: Principles and Design*, 3rd ed.; John Wiley &Sons, Inc: New York, 2012; pp 1861−1862.

DOI: 10.1021/acs.jpcb.9b06038
J. Phys. Chem. B XXXX, XXX, XXX−XXX